- Technical Paper-

PHASES ANALYSIS ON FLY ASH CONCRETE BY USING SYNCHROTRON X-RAY COMPUTED MICROTOMOGRAPHY

Ivan S. DARMA[*1], Takafumi SUGIYAMA[*2], Takashi HITOMI[*3], Kazunori SHIMURA[*4]

ABSTRACT

This paper reveals the usage of Synchrotron X-Ray Computed Tomography to determine different phases of the microstructure of fly ash concrete. The fly ash mortar specimen was prepared with a size of 1 mm ×1 mm × 15 mm to obtain microtomographic images with a spatial resolution of 0.5 μm/voxel. The observation of specimen was conducted not only in static condition but also in applied load condition. Volume and area fraction of each phase were determined. In addition, a method to estimate the stress and the modulus of elasticity of the mortar was provided in this research.

Keywords: synchrotron X-Ray CT, microstructure, fly ash mortar, elastic modulus, stress distribution

1. INTRODUCTION

At a microscopic level, the complexities of concrete microstructure are evident. This is because it is neither homogeneously distributed with respect to each phase present in the structure nor they themselves homogeneous. In order to develop new cementitious materials the roles of each different phase present in the microstructure of concrete subjected to either external or internal forces must be clarified. However, without quantitative evaluation with respect of volume and area fraction of each phase at a microscopic level the behavior of concrete under study is hardly discussed in details.

Recently the SPring-8 (Super Photon ring-8 GeV) has been used to explore the microstructure of a cementitious material from viewpoints of a 3D rendering [1-4]. It is expected through this instrument we may identify and classify not only voids but also each phase at a given microstructural level in concrete specimen. Research with the imaging technique is currently limited according to its resolution although advantage of the usage of this instrument is highly admitted for studies on cementitious materials.

In this paper, different phases in the microstructure of mortar specimen are revealed in form of hydrated cement paste, unhydrated cement grains, fly ash, voids and aggregates of microstructure. In addition, based on the results of the phase separation stress level distribution in the mortar is also presented as an impact of load application.

2. METHODS

2.1 Sample preparation

Table 1 shows a set of mixture proportions used for microtomography study. Ordinary Portland Cement (OPC) and JIS type II fly ash are used as a binder material. Replacement of fly ash for OPC ratio is 0.15 by mass, while water to cement ratio (w/c) is fixed at 0.58.Fresh mortar was placed into the mold in a size of 40 x 40 x 160 mm and cured in water for 28 days.

Table 1 Mix proportion for microtomographic study

Item	Unit weight (kg/m^3)
Portland Cement	578
Water	340
Fine Aggregate	1020
Fly ash	102
Water Reducer Admixture	1.73

Table 2 Chemical compositions of fly ash

Chemical Composition (%)										
SiO_2	Al_2O_3	Fe_2O_3	CaO	MgO	Na_2O	K_2O	SO_3	TiO_2	MnO	Others
66.42	18.88	3.63	0.90	0.54	0.04	1.23	0.15	0.82	0.03	7.36

Fig.1 A set of samples for microtomography study

*1 Ph.D Student, Graduate School of Engineering, Hokkaido University, JCI Member
*2 Professor, Faculty of Engineering, Hokkaido University, JCI Member
*3 Senior Researcher Engineer, Technical Research Institute, Obayasi Corp, JCI Member
*4 Assistant Professor, Faculty of Engineering, Hokkaido University, JCI Member

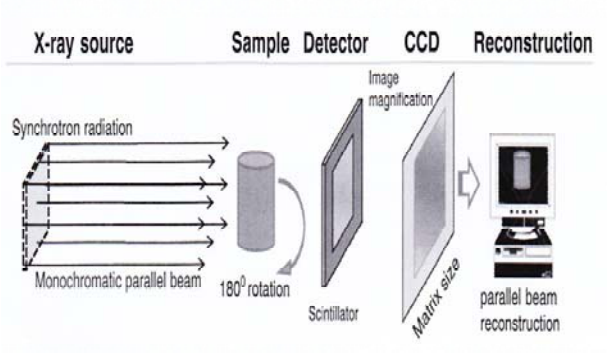

Fig.2 X-ray CT system in SPring-8

After 28 days curing periods, mortar is cut to obtain a sample size of 1 mm x 1 mm no less than 15 mm in length. Aggregates with a diameter of less than 0.5 mm are utilized to avoid the possibility of cross section along the specimen is dominated by the aggregate.

2.2 Synchrotron X-Ray CT

In this study, BL20XU beamline at SPring-8, which is the world's largest third generation synchrotron radiation facility, was used to obtain set of CT slices/images. A schematic illustration of X-Ray imaging system at SPring-8 is shown in Fig.2. The system consists of an X-Ray light source from the beam line, double crystal monochromator, high-precision rotation stage, and high-resolution X-Ray image detector [5]. The transmitted images are detected by X-Ray imaged detector that consists of a thin scintillator, optic system and CCD camera. For each specimen, 1500 X-Ray projection images with an angle step of 0.12 degrees and an exposure time of 0.3 s each ware obtained.

The beam energy was set to a value of 25 keV to obtain 1300 contiguous grayscale images, which each slice image contained 2000 x 2000 voxel. The dimension of a voxel is a 0.5 x 0.5 micrometer-sized pixel with a thickness of 0.5 µm. Thus, the effective size of the cubic voxel is 0.5 µm in the CT image.

The microtomographic images produced were determined from each of the elements' attenuation coefficients. Attenuation coefficient of a material can be defined as the rate at which it absorbs energy from a ray. This leads to the theory behind the scan which illustrates that denser material will have higher linear attenuation coefficient (μ) values and absorbs more energy. Therefore a CT scan is a map of the spatial distribution of μ values which reveals the different in density within the object. Images are typically scaled so that brightness is proportional to X-ray absorption, thus bright regions corresponds to high density phases while dark region would correspond to low density phases. A hole or pore space in a sample would appear to be practically black.

From previous studies, a list of theoretical linear attenuation coefficient (LAC) of different phases in hardened cement paste has been calculated based on mass attenuation coefficient at X-ray energy level of 15 keV, which was obtained from NIST database [2]. By using the same method, the theoretical LAC of different phases in hydrated cement system at X-ray energy level of 25 keV could be determined.

2.3 Image enhancing technique

There are many methods that can be applied to obtain enhanced images. However, to choose which methods will be used should depend on the objectives of the study. In this study, the objective to be achieved is to detect and separate any solid phases present in fly ash mortar based on histogram. Then among other a "mean" filtering method was chosen with 7 pixels in radius.

Fig.3 shows the different image and histogram before and after enhancing process. In original image histogram, there is one peak value of LAC which means one solid material exists. However, there are two kinds of solid materials in it visually. First, the darker one represents lower density material and the brighter represents higher density material. After enhancing process beside smoother image, new histogram also obtained. This histogram shows clearly that there are two peak values of LAC which represent two solid materials as shown visually.

2.4 Separation of each phase

The method that used to classify each solid phase in this microtomography study is combining both histogram analysis and theoretical LAC. Fig.4 shows how to separate each phase in a mortar histogram. Through the peaks, we could make two new curves with approach of polynomial equation level 2. Each curve has its solution, which will become a threshold. However, in this case the two curves intersect; the intersection point will become threshold for each other. From this point, we may have pore phase from 0 to α_1; Solid phase 1 from α_1 to α_i and the last solid phase 2 from α_i to α_4. By referring this range of threshold to theoretical LAC**,** information about kinds of those phases will be obtained.

To avoid possible edge effect and reduce the computing time, a region of interest (ROI) was selected, and a cubic volume of interest (VOI) was obtained as well. In this study, the VOI was limited to 1000 × 1000 × 1000 voxel.

2.5 Tensile load application

In this study the specimen was not only observed in static conditions, but also in applied load condition. Fig.5 shows the instrument used in the application of tensile force. Electrical energy that flows into the piezoelectric actuator is converted into a force that propels the lever above it. Furthermore, due to the movement of the tip of the lever toward the top, then the other end of the lever will move downward. Downward movement of the lever becomes the tensile force which is applied to the specimen. The amount of force applied will be read by a load cell which is above the piezoelectric.

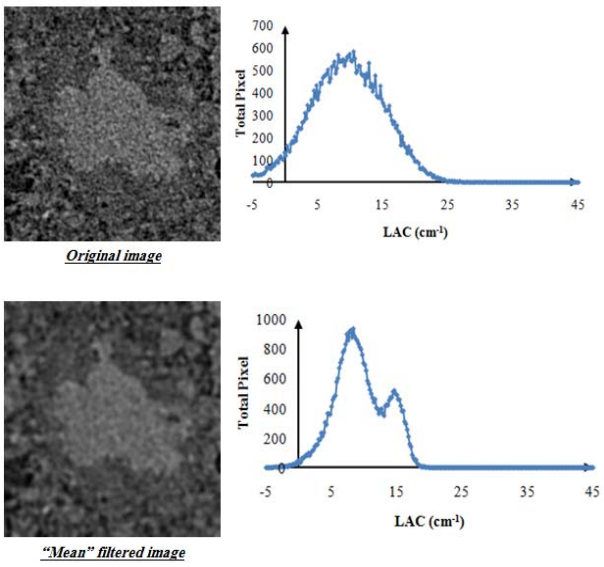

Fig.3 Example of image and histogram before and after enhancing process

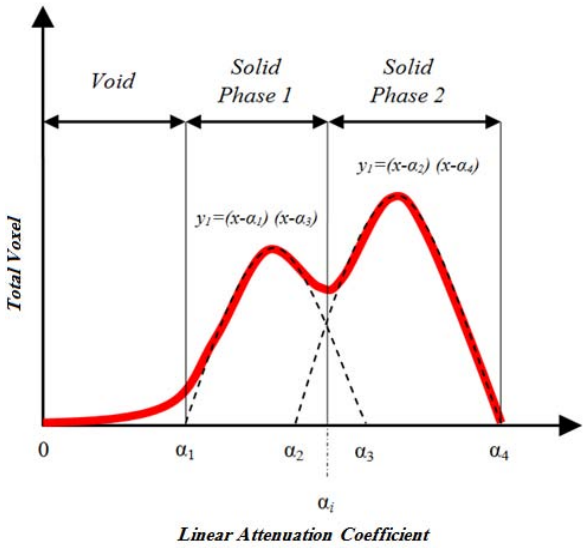

Fig.4 Example of mortar histogram

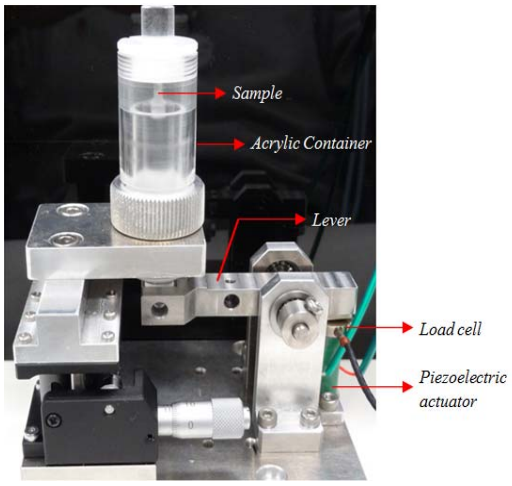

Fig.5 Micro-tensile test instrument

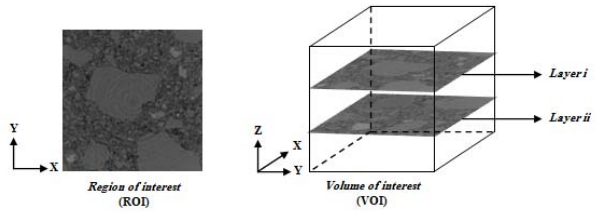

Fig.6 Layers combination to determine stress of each phase

In microscopic level, concrete can be classified as inhomogeneous material which has several phases. Therefore, when this material is subjected to load, the stress will vary from one phase to another phase. In this study, we assumed that hydrated cement pastes and aggregates are the load bearing phases. Fig.6 shows the illustrative to determine level of stress of each load bearing phases using equations given below.

$$P_{VOI} = (\sigma_{HCP} A_{HCP}) + (\sigma_{Agg} A_{Agg}) \quad (1)$$

$$Layer\ i \rightarrow P_{VOI} = (\sigma_{HCP-i} A_{HCP-i}) + (\sigma_{Agg-i} A_{Agg-i}) \quad (1a)$$

$$Layer\ ii \rightarrow P_{VOI} = (\sigma_{HCP-ii} A_{HCP-ii}) + (\sigma_{Agg-ii} A_{Agg-ii}) \quad (1b)$$

where,

P	: load
σ	: stress
A	: sectional area
HCP	: hydrated cement paste phase
Agg	: aggregate phase

3. RESULTS AND DISCUSSION

3.1 Image analysis of phase identification

Fig.7 describes the representative slices obtained from specimen after normalization process. As shown in this figure, the background is imaged as very dark voxel in contrast to the foreground or scanned object. As explained before, the darker voxel in the reconstructed grayscale image correspond to low density phases (e.g., air voids or pores), whereas the brighter voxel denote the high density phases (e.g., anhydrous cement). In microtomographic images of the mortar, from medium to the dark grey voxel that are distributed in all over the cross-section are most likely associated with the hydrated cement products. On the other hand, the light to the medium voxel are represented the fine aggregate.

Fig.8 shows the histogram of volume of interest (1000×1000×1000 voxel). Visually, there are 4 peaks in the curve and each peak definitely represents each solid phase in mortar. By using separation method as described in 2.4, it is known that these phases are hydrated cement paste, fine aggregate, unreacted cement grains and unhydrated fly ash grains. The LAC threshold for each phase is shown in Table.3 as the reference of the theoretical LAC given in Table 4.

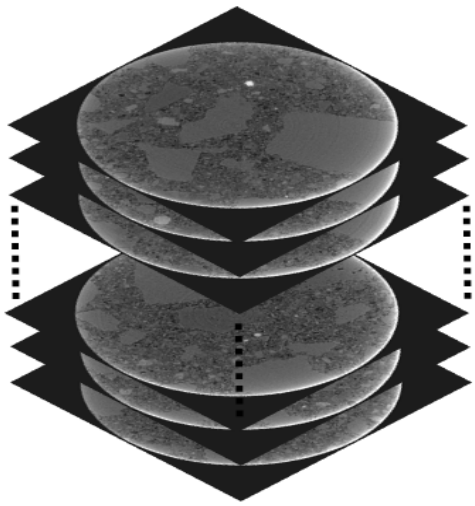

Fig 7 Cross-sectional slices with the normalized reconstructed 8-bit grayscale image (2000×2000 voxel of 0.5 µm)

Subsequently, by using Table 4 as a reference; it is known that in a segmented phase contains several solid phases. For example, hydrated cement paste phase, which has a threshold value of LAC from 5.82 to 9.80. Within this threshold, there are LAC values for two main solid phases of hydrated cement product comprises CSH (8.31) and CH (9.08).

However, due to the fact that LAC value of hydrated cement products are very close; it is very difficult to separate any phases in hydrated cement products. It is also occurred to the unhydrated cement grains phase, which has a threshold 12.37 to 16.26where within this threshold another solid phases in cement grains could be identified such as C_3S, C_2S, C_3A and C_4AF.

In addition, 3-dimension of separated phases is shown in Fig.9. From this figure we can see how each solid phase disperse in a volume of interest of hardened mortar. This research also reveals the geometry of the particles of fly ash in the mortar. Two types of fly ash particles were detected in mortar. First, fly ash particles which have reacted. Second, fly ash particles which may not have reacted in form of a cenosphere and fly ash grains. Fig.10 shows the fly ash particle which may react and hydrate. This is because based on LAC value, inner of the hydrated sphere appears to be similar with hydrated cement paste phase.

Fig.11 shows the incomplete reacted fly ash particle in form of cenosphere. Visually, microtomographic image of cenosphere is similar to sphere with 2 µm high density shell thickness surrounding a cavity. However, based on LAC histogram the cavity might be a phase of Mullite and quartz which has lower density compared with the shell that surrounds the cavity. Fig.12 shows unreacted fly ash particle in the form of sphere with a high density level. Magnetite and Hematite phases may contribute to the high density level of unreacted fly ash particle.

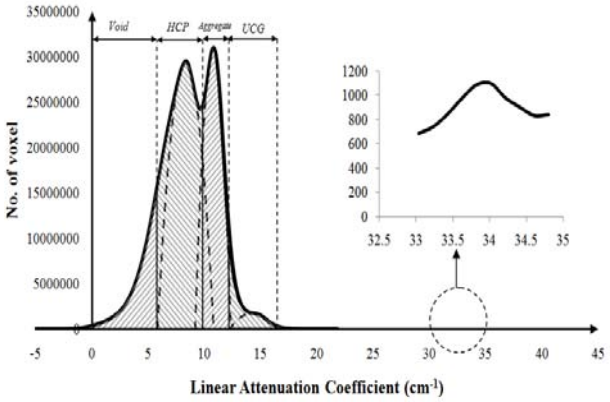

Fig.8 Microtomographic images histogram

Table 3 LAC Threshold for each phase

Phase	LAC (cm^{-1})			Volume Fraction
Void	-5.00	-	5.82	0.12
Hydrated Cement Paste	5.82	-	9.80	0.51
Aggregate	9.80	-	12.37	0.32
Unhydrated Cement Grain	12.37	-	16.26	0.04
Unhydrated Flyash Grain	33.06	-	34.79	9.0E-06

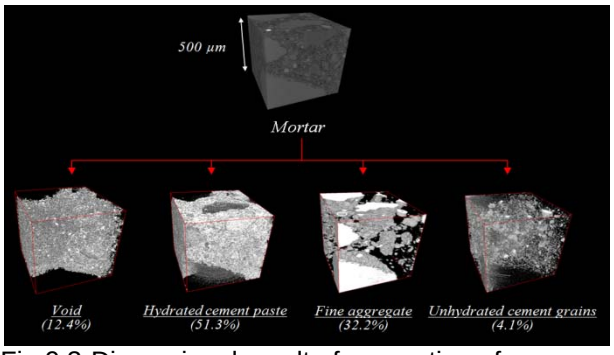

Fig.9 3-Dimensional result of separation of any phases in mortar specimen

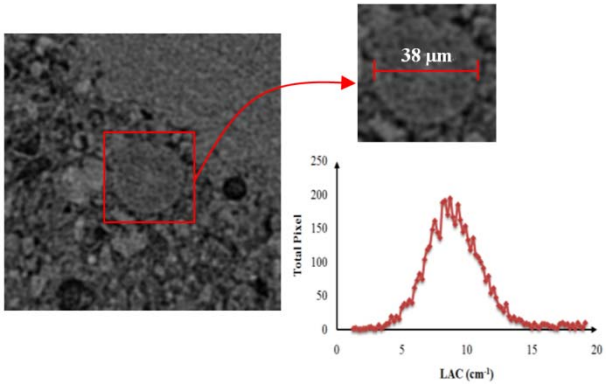

Fig.10 Fly ash that may react in microtomographic image

Table 4 Theoretical linear attenuation coefficient of different phases in hardened cement paste

Phase	Chemical Formula	Notation	LAC (cm^{-1}) at 15 keV (Promentilla *et al.*, 2008)	LAC (cm^{-1}) at 25 keV
Magnetite	Fe_3O_4	F_3	-	51.91
Hematite	Fe_2O_3	F_2	-	51.05
Ferrite	$(CaO)_4(Al_2O_3)(Fe_2O_3)$	C_4AF	91.16	21.84
Free Lime	CaO	C	72.45	17.14
Alite	$(CaO)_3(SiO_2)$	C_3S	56.51	13.47
Belite	$(CaO)_2(SiO_2)$	C_2S	53.24	12.73
Aluminate	$(CaO)_3(Al_2O_3)$	C_3A	46.97	11.25
Portlandite	$Ca(OH)_2$	CH	37.91	9.08
Calcium Silicate Hydrate	$(CaO)_{1.7}(SiO_2)$ $1.8H_2O$	C-S-H	34.37	8.31
Gypsum	$CaSO_4$ $2H_2O$	$C\bar{S}H_2$	25.19	6.28
Calcium Silicate Hydrate	$(CaO)_{1.7}(SiO_2)$ $4H_2O$	C-S-H	23.76	5.82
Monosulfate	$(CaO)_3(Al_2O_3)(CaSO_4)$ $18H_2O$	$C_4A\bar{S}H_{12}$	20.33	4.40
Mullite	$3Al_2O_3.2SiO_2$	A_3S_2	-	4.38
Quartz	SiO_2	S	-	3.86
Ettringite	$(CaO)_3(Al_2O_3)(CaSO_4)_3$ $32H_2O$	$C_6A\bar{S}_3H_{32}$	14.33	3.59
Water	H_2O	H	1.68	0.59
Air	-	-	0.002	0.001

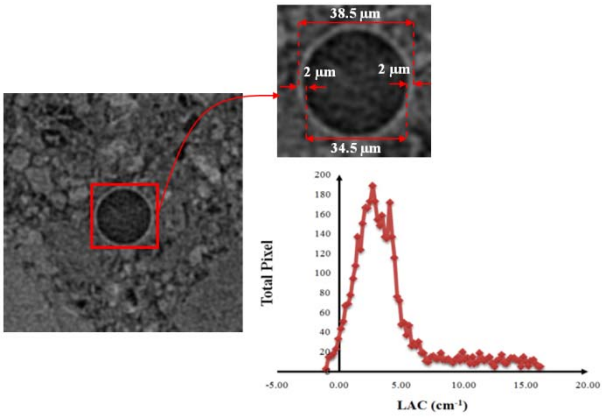

Fig.11 Cenosphere in microtomographic image

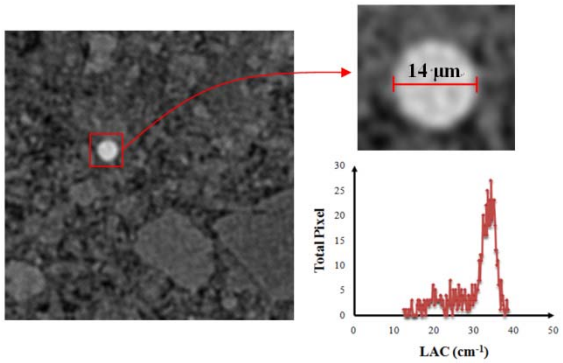

Fig.12 Fly ash that may not have reacted in microtomographic image

3.2 Stress distribution

Fig.13 shows the relationship of stress level of load bearing phases (cement paste and aggregate) along the specimen length at maximum load of 4.3N. The stress is the calculated with Eq.(1) by using some combination between the two layers. Basically, the level of stress is strongly influenced by the surface area of each phase. The larger the area of a phase has, the higher stress is occurred. Furthermore, higher percentage load is borne by this phase.

Subsequently, the probability stress level at each solid phase in the mortar at a maximum load is shown in Fig.14. For the cement paste phase, the average stress level resulting from the maximum load of 4.3N is equal to 5.6 MPa with a standard deviation value of 0.79 MPa. As for the aggregate phase, the average stress level at maximum load 4.3N is equal to 4.5 MPa with a standard deviation value of 1.08 MPa.

This approach will help the development of a new inclusion in cementitious material under consideration because relative stress levels of each phase present in the material can be estimated.

3.3 Modulus of elasticity

The main factor that determines the value of modulus of elasticity is the elasticity modulus and sectional area of each phase (cement paste and aggregate). The moduli of sand (E_{Agg}) are taken as the typical values for a sandstone or quartz-rich rock [6] approximately 88.7 GPa. While elastic modulus of cement paste (E_{CP}) as much as 12 GPa is utilized [7]. Subsequently, by using equation below the modulus of elasticity of mortar (E_c) could be determined.

$$E_C = \frac{\left(E_{Agg} \times A_{Agg}\right) + \left(E_{CP} \times A_{CP}\right)}{A_{Total}} \qquad (2)$$

Since in a VOI there are 1000 layers then we may have 1000 values of *Ec* obtained from equation above. Fig.15 shows the probability distribution of elastic modulus of VOI in mortar samples. The mean value of modulus of elasticity obtained from this study equals 34.7 GPa with a standard deviation value of 5.2 GPa.

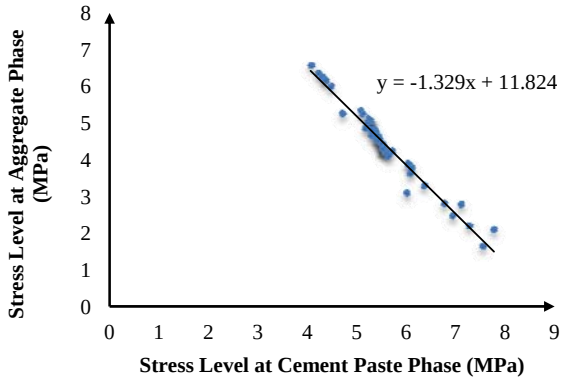

Fig 13 Relationship of stress level of each phase

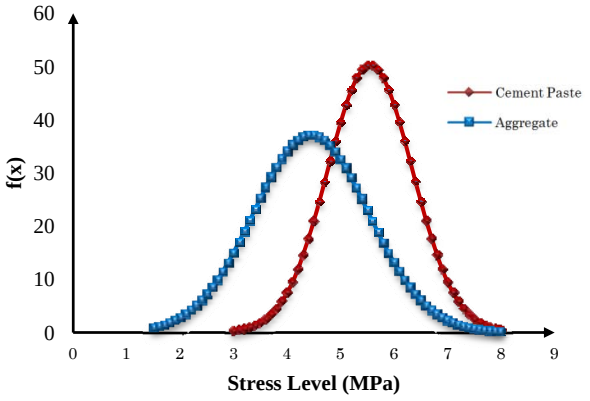

Fig.14 Probability distribution of stress level of each phase at maximum load of 4.3N

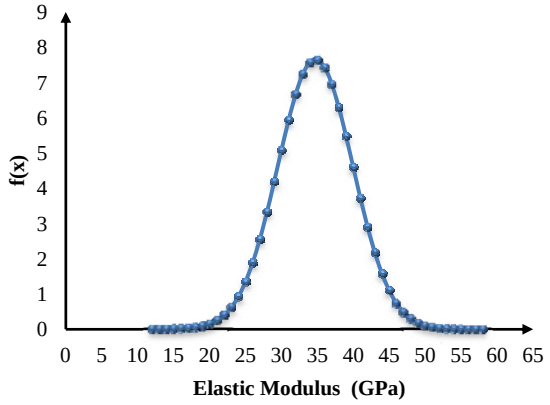

Fig.15 Probability distribution of modulus of elasticity of mortar

4. CONCLUSION

Based on the results of this research, the following conclusions are being drawn as follows:

(1) Synchrotron X-Ray CT can be used not only to determine volume of voids, but also to detect and separate any solid phases in the microstructure of mortar in form of hydrated cement paste, aggregate and any grains.
(2) Relative stress levels of each phase present in the material as the result of load applied can be estimated.
(3) A method to estimate of mechanical properties of multiphase material is provided.

ACKNOWLEDGEMENT

Part of this present research was founded by the Japan Society for Promotion of Science (Research No. 23360187). The synchrotron radiation experiments were performed at the BL20XU in SPring-8 with the approval of the Japan Synchrotron Radiation Research Institute (JASRI) (Proposal No.2011A1260).

REFERENCES

[1] Hitomi, T., Mita, Y., Saito, H. and Takeda, N. “Observation of fine structure of mortar using X-ray CT images in SPring-8,” In: Proceeding of the Japan Concrete Institute, 26(1), 645-650, 2004
[2] Promentilla M.A.B., Sugiyama T., Hitomi T., Takeda N., “Characterizing the 3D Pore Structure of Hardened cement Paste with Synchrotron Microtomography,” Journal of advanced Concrete Technology, Vol.6, No.2, pp.273-286, 2008
[3] Sugiyama T.,Promentilla M.A.B., Hitomi T., Takeda N., “Application of synchrotron microtomography for pore structure characterization of deteriorated cementitious materials due to leaching,” Cem. Con. Res. Vol.40, pp.1265-1270, 2010
[4] Promentilla M.A.B., Sugiyama T., Hitomi T., Takeda N., “Quantification of tortuosity in hardened cement pastes using synchrotron-based X-ray computed microtomography,” Cem. Con. Res.Vol.39, pp.548-557, 2009
[5] Uesugi, K., Suzuki Y., Yagi, N., Tsuchiyama, A. and Nakano, T. (2001). “Development of high spatial resolution X-Ray CT system at BL47XU in SPring-8,”*Nuclear Instrument and Methods I Physics Research A*, 467-468, 835-856
[6] Kuster, G.T., Toksoz, M.N., “Velocity and attenuation of seismic waves in two-phase media: Part II. Experimental Results,” Geophysics 39 (5), 587-606, 1974b
[7] Anson, M., and Newman, K. “The effect of mix proportions and the method of testing on Poisson’s ratio for mortars and concrete,” Mag. Of Concrete Res., 18, 115-130, 1966